Lab on a Chip

An Ultra High-Efficiency Droplet Microfluidics Platform Using Automatically Synchronized Droplet Pairing and Merging

Journal:	*Lab on a Chip*
Manuscript ID	LC-ART-07-2020-000757
Article Type:	Paper
Date Submitted by the Author:	28-Jul-2020
Complete List of Authors:	Zhang, Han; Texas A&M University System, Electrical and Computer Engineering Guzman, Adrian; Texas A&M University, Electrical and Computer Engineering Wippold, Jose; Texas A&M University System, Biomedical Engineering; Li, Yuwen; Texas AandM University, ECE Department Dai, Jing; Texas A&M University, Electrical and Computer Engineering Huang, Can; Texas A&M University System, Electrical and Computer Engineering Han, Arum; Texas AandM University, ECE Department

Lab on a Chip

PAPER

An Ultra High-Efficiency Droplet Microfluidics Platform Using Automatically Synchronized Droplet Pairing and Merging

Received 00th January 20xx,
Accepted 00th January 20xx

DOI: 10.1039/x0xx00000x

Han Zhang, [1]‡ Adrian Guzman, [1]‡ Jose Wippold, [2] Yuwen Li, [1] Jing Dai, [1] Can Huang, [1] Arum Han, [1,2]*

Droplet microfluidics systems hold great promise in their ability to conduct high-throughput assays for a broad range of life science applications. Despite their promise in the field and capability to conduct complex liquid handling steps, currently, most droplet microfluidic systems used for real assays utilize only a few droplet manipulation steps connected in series, and are often not integrated together on a single chip or platform. This is due to the fact that linking multiple sequential droplet functions within a single chip to operate at high efficiency over long periods of time remains technically challenging. Considering sequential manipulation is often required to conduct high-throughput screening assays on large cellular and molecular libraries, advancements in sequential operation and integration are required to advance the field. This current limitation greatly reduces the type of assays that can be realized in a high-throughput droplet format and becomes more prevalent in large library screening applications. Here we present an integrated multi-layer droplet microfluidic platform that can handle large numbers of droplets with high efficiency and minimum error. The platform combines two-photon photolithography-fabricated curved microstructures that allow high-efficiency (99.9%) re-flow of droplets and a unique droplet cleaving that automatically synchronizes paired droplets enabling high-efficiency (99.9%) downstream merging. We demonstrate that this method is applicable to a broad range of droplet sizes, including relatively large droplet sizes (hundreds of micrometers in diameter) that are typically more difficult to manipulate with high efficiency, yet are required in many cell assay applications requiring large organisms or multiple incubation steps. The utility of this highly efficient integrated droplet microfluidic platform was demonstrated by conducting a mock antibiotic screening assay against a bacterial pathogen. The approach and system presented here provide new avenues for the realization of ultra-high-efficiency multi-step droplet microfluidic systems with minimal error.

1. Introduction

Droplet microfluidic systems utilize a high-throughput emulsification process to produce monodispersed water-in-oil emulsion droplets that function as individual pico-liter-volume bioreactors. These droplets, which can encapsulate various target materials such as reagents, cells, and microbeads, can be handled and manipulated at extremely high throughputs. The advantages of high-throughput, small-volume, and single-cell/single-bead manipulation inherent to this technology provides substantial advantages over conventional robotic liquid handling or other continuous flow microfluidic-based approaches.[1-6] Almost all liquid handling steps can be now performed in droplet format, such as droplet generation, droplet merging, droplet splitting, droplet detection, droplet sorting, and in-droplet cell/bead manipulation, to name a few. These functions and systems have now been extensively developed and utilized in a broad range of life science applications, both for cell-based and cell-free assays.

However, three major challenges remain that prevent droplet microfluidic systems from being adopted for a broader range of applications and more complex multi-step assays. First, many biological assays require multiple liquid-handling steps to be conducted in a sequential manner. Despite the fact that droplet microfluidics technology can conduct almost all liquid handling steps in droplet format, linking more than a few droplet manipulation steps in series, especially on a single chip, remains a major challenge. This is because any error in an assay step adds to the overall system error (e.g., sequentially linking just two steps, each having 5% error rate, results in an overall system error rate of 9.75%), thus the overall system efficiency becomes exponentially lower as the error rates compound. This is especially problematic in high-throughput library screening applications where droplet microfluidic systems can be extremely powerful, since high error rates would mean that a very large number of potential “hits” have to be re-tested (false-positive case) or a large number of potential “hits” would be lost (false-negative case). Thus, minimizing the error rate in every droplet manipulation step becomes critical. Amongst the many droplet manipulation steps, droplet merging remains a critical

[a] Department of Electrical and Computer Engineering, Texas A&M University, College Station, Texas 77843, USA.
[b] Department of Biomedical Engineering, U Texas A&M University, College Station, Texas 77843, USA.
‡These authors contributed equally to this work and should be considered co-first authors.
Electronic Supplementary Information (ESI) available: [details of any supplementary information available should be included here]. See DOI: 10.1039/x0xx00000x

bottleneck in this regard. Second, having to process large libraries for assays requiring several hours of cultivation, which is the case in many biological assays, means that the system has to operate with high efficiency for long periods of time (e.g., tens of hours). Many droplet microfluidics systems developed thus far, especially those that link more than just a few droplet manipulation steps in series, typically cannot run stably for long periods of time. Limitations in such long-term stability often stem from unstable reflow of droplets. Differences in droplet-to-droplet distances and loosely packed droplets that are being re-flown all have a direct negative impact on the efficiency of downstream droplet handling steps, such as droplet synchronization and merging. Third, many cell-based assays require cultivation and/or incubation steps of several hours (sometimes even tens of hours), and thus to avoid nutrient limitation, a sufficient droplet volume or replenishment is needed. However, the smaller the droplet sizes are, the more stable the droplets are, and thus enable faster and more efficient droplet operation. As the droplet size increases to beyond 50 – 100 μm in diameter, droplets become more unstable especially when manipulating the droplets at high speeds, often resulting in unexpected droplet shearing, droplet splitting, and droplet merging. Taken together, significant advances in various droplet manipulation techniques and serial operations are still needed to harness the full potential of droplet microfluidic approaches.

Two aspects that can overcome many of the above-mentioned challenges are related to merging two different liquid samples, mainly in the form of droplet reflow and droplet merging steps. Many droplet pairing and merging techniques have been developed so far,[7-11] but linking more than a few droplet manipulation steps in series in an integrated chip format remains a major challenge.[12] When two droplets have to be merged one-to-one into a single droplet, first pairing them one-to-one before merging is the most critical step to ensure all droplets are merged at a one-to-one ratio with high efficiency (i.e., no unmerged droplets or no three or more droplets merged into a single droplet). Various pressure-equilibrating structures such as micropillar arrays, railroad-like microfluidic channel structures, and pressure oscillators/regulators have been employed to improve the pairing efficiency so that two trains of droplets to be merged are first paired with each other,[8-10] However, droplets do not always enter such synchronization region in an orderly manner, often resulting in low pairing efficiency (less than 90%).[8-10] Other methods such as utilizing two different sizes of droplets so that one droplet catches up to the other droplet can also increase the pairing efficiency,[11] but the efficiency still relies on how consistent the incoming droplet flow can be maintained. Overall, in almost all of these methods, the droplet merging efficiency remains in the range of 80 - 95%, especially when looking at the long-term efficiency (e.g., for hours). Considering an optimum scenario of 95% pairing/merging efficiency, when linking two such merging schemes in series, the overall system efficiency drops to approximately 90%, meaning that when processing a library of 1 million cells, 100,000 droplets will potentially be false positives and/or false negatives. If the merging efficiency is 99%, this still means that about 10,000 cells will be false positives/false negatives, a very large number to be re-tested and re-confirmed.

Second, regardless of the method used, stable and consistent flow of droplets are critical in maintaining high droplet pairing and merging efficiencies. However, this is non-trivial, as any sudden changes in droplet flow direction in the microfluidic system or droplets moving from a chip to tubing and/or vice versa can cause inconsistent droplet reflow and introduction into the merging region.[13] In these cases, variations in droplet-to-droplet distances, droplet shearing, droplet splitting, and droplet merging at interfacial junctions are often observed, resulting in low droplet pairing and merging efficiencies. Integrating all droplet functions onto the same chip can minimize issues stemming from device-to-tubing interfaces, but due to inherent sharp corners often present in conventional microfluidic channel structures, abrupt changes in the droplet flow speed/direction cause high shear stress conditions that lead to low efficiency operation.[14] For example, re-flowing droplets from a densely packed vertical droplet culture reservoir into a channel[15] requires droplets to make a sudden change in flow direction while they also undergo movement from a large channel to a small channel. Thus, a system that can provide the means to re-flow droplets highly consistently under very stable flow conditions so that all droplets flow into the droplet pairing/merging region at the same flow speed and with the same droplet-to-droplet distance is critical in having high-efficiency droplet pairing and merging.

Alternative to such droplet synchronization and merging method, another method that allows combining two different liquid samples into a single droplet is the “pico-injection” technology.[16, 17] This method utilizes a pressurized aqueous flow channel positioned perpendicular to the droplet flow channel to inject a controlled volume of reagent directly into each droplet that is passing by the injection orifice using an electric field. This eliminates the need for first generating a droplet to be merged and then having to pair them to the incoming droplets before they are merged together. Because two steps are combined into a single step, the simplicity of this method and the elimination of the need for droplet synchronization is a major advantage. However, there are also several limitations to this method, where the volume of solution that can be injected into the solution is typically only a fraction of the incoming volume and thus a larger volume cannot be injected, whereas such operation is needed in many biological assays.[18-21] Since the injection orifice has to be relatively narrow (5 – 20 μm range[22-28]), adding large objects such as microbeads and cells are difficult. Also, imperfect injection can lead to cross-contamination issues at the injection orifice,[26, 27, 29] and the occasional injection of solution into the main channel as small droplets can cause false positive/negative signals during the downstream droplet detection step. In general, this method also relies on the droplets being reflowed very consistently to achieve high efficiency.

Here, we describe the development of a droplet manipulation process entailing droplet generation, large-volume first-in-first-out droplet cultivation, controllable droplet reflow, on-the-fly

droplet cleaving to generate a pair of droplets that are automatically paired and do not require an additional synchronization step, and droplet merging, all at an ultra-high efficiency. Two fundamental innovations are enabling this: the use of curved microstructures (in both planar and vertical directions) that allow droplet reflow to be consistent without any sudden change in flow characteristics, and a new droplet cleaving scheme where water-in-oil emulsion droplets flow into a continuous aqueous-phase flow and cleave the flow into another set of water-in-oil emulsion droplets so that the two droplets are automatically paired with each other. Here, the curved microstructures are produced by two-photon photolithography (2PP) microfabrication. Such structures are not achievable using conventional lithography steps. Using the proposed scheme, a consistent droplet pairing and merging efficiency of 99.9% was obtained, and the same efficiency was also achieved for the overall integrated droplet microfluidic system developed. The approach developed herein offers the ability to conduct large-scale multi-step droplet processing at an unprecedented efficiency and with a corresponding low error rate, and entails a novel technique that can be broadly applied to pair two (or more) droplets at varying sizes and ratios, all at an extremely high efficiency.

2. Materials and Methods

2.1 Device design and operating principle

The two main innovations driving the presented droplet microfluidics system are: the use of both planar- and vertical-direction curved microstructures to minimize abrupt changes in droplet flow directions to minimize droplet shear stress, enabling consistent droplet reflow; and a method where a water-in-oil emulsion droplet is cleaving an aqueous solution flow to generate a second water-in-oil emulsion droplet that is accurately and automatically paired (in one-to-one ratio) and synchronized. Fig. 1a shows a cross-section view where droplets packed in a vertical droplet cultivation chamber are reflowed and smoothly transition to a planar droplet reflow channel while all droplets remain tightly packed, thus providing a method for consistent droplet reflow with constant droplet-to-droplet distances and droplet flow speed. These vertically curved microstructures were fabricated using a 2PP technique, described in detail in section 2.2. Fig. 1b shows the droplet cleaving and auto-pairing/synchronization scheme, where a train of water-in-oil emulsion droplets flow into an aqueous solution flow stream, allowing the carrier oil surrounding the first droplet train to cleave the aqueous solution and generates a second water-in-oil emulsion droplet from the aqueous solution. This results in the first droplet and the newly cleaved droplet to be paired and remains in close proximity to one another, making downstream droplet merging highly efficient. If the droplet-to-droplet distance of the first droplet train is within a certain range (various conditions described in more detail in the results section), this always generates only a single cleaved droplet, allowing close to 100% one-to-one ratio droplet generation and pairing. In addition, as long as the first droplet train flows in with minimum variation in droplet-to-droplet distances (enabled by the above-described droplet reflow scheme), consistent droplet pairing can be achieved. These paired droplets can then be flown through a meandering droplet merging channel where two parallel 3D electrodes are used to merge the paired droplets through the induction of an electric field (Fig. 1c).

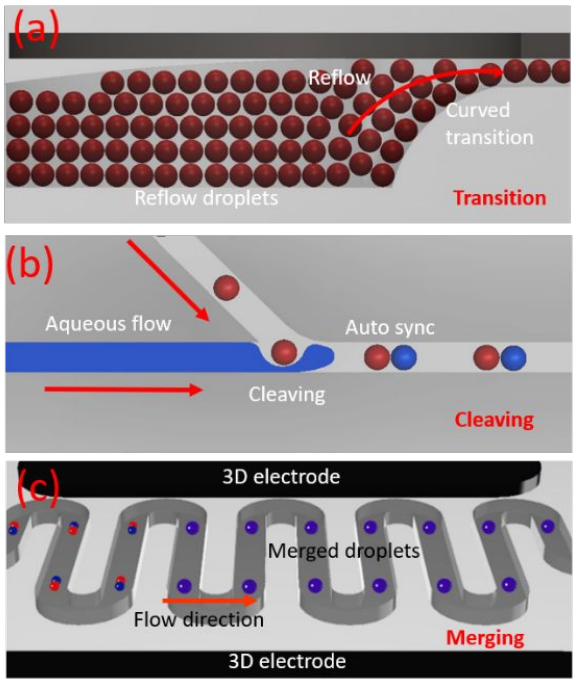

Fig. 1 Schematic of the (a) curved microstructure-enabled droplet transition junction, (b) droplet cleaving and auto-synchronization structure, and (c) electrocoalescence-based droplet merging zone using a pair of 3D electrodes.

These two innovations are incorporated into a droplet microfluidic system designed to perform a typical co-cultivation based high-throughput screening assay, such as the investigation of polymicrobial interactions of cells or drug screening applications typically comprising large library screening endeavours (Fig. 2). Fig. 2a shows the overall workflow of such an assay, where droplets encapsulate cells or molecules of interest from a large library to create a droplet library, in some cases these droplets are incubated first for several hours (e.g., microbe-encapsulated droplets producing biochemicals of interest that needs to be screened), another train of droplets encapsulating target cells are generated, these two droplets are then merged and cells are co-cultivated, followed by an analysis of changes to the target cells, and sorting of the droplets of interest (if needed). A requirement to enable all of these steps in a single integrated format is the integration of a relatively large droplet cultivation chamber (typically at least several millimetres in scale), since the target applications typically require processing large libraries, where a planar droplet cultivation chamber cannot accommodate such large number of droplets. With these constraints in mind, a platform that consists of 5 layers integrated into a single system was designed. The working principle of the entire system,

including droplet generation, reflow, cleaving, merging, and co-cultivation is shown in Fig. 2b. Since the main focus of this work is to demonstrate the advantages that the novel high-efficiency droplet reflow and merging scheme can bring to droplet microfluidic systems, this version of the platform did not include a droplet sorting function.

Fig. 2c, d and e show the exploded 3D view of each layer of the system, the aerial view, and the top view of the system, respectively. The blue color structures indicate the fluidic channels and the gold color structures indicate the 3D electrodes (width: 250 µm). 3D electrodes were used here to provide a more uniform and stronger electrical field while supplying a lower voltage when compared with conventional two-dimensional electrodes.[30] On each side of the 3D electrodes, four shielding electrodes (width: 250 µm) are positioned to prevent the electric field from radiating to other parts of the system and causing unwanted droplet merging.

From bottom to top, the heights of the microfluidic channels and droplet cultivation chambers embedded in each layer are: 50 µm for the bottom droplet generator layer (L1 in Fig. 2c), 6 mm for the droplet culture chamber layer (L2 in Fig. 2c), 200 µm for the curved droplet transition channel layer (L3 in Fig. 2c), 50 µm for the droplet cleaving/auto-synchronization/merging channel layer (L4 in Fig. 2c), and 50 µm for the valve layer (L5 in Fig. 2c) controlling the droplet reflow. The bottom-most layer (L1) contains the first droplet generation microstructure utilizing a cross-junction shaped droplet generator having channel dimensions of 50 µm × 50 µm. The second layer from the bottom (L2 in Fig. 2c) is a vertical chamber with an approximate volume of 0.052 ml for droplet storage and incubation. Additionally, the design and operating scheme offer first-in first-out droplet reflow where the inlet is located at the bottom and outlet is located at the top so that droplets float upwards due to the density difference between the aqueous solution (1 kg/L) and carrier oil (Novec oil 7500 3M™, Saint Paul, MN, USA; 1.614 kg/L). This allows all droplets to undergo equal incubation times, as reported previously[15]. The cone shape of this droplet cultivation chamber (bottom radius: 3 mm, top radius: 0.5 mm) was designed to prevent an abrupt change in the droplet flow and to minimize the dead volume. After collection of the droplets in this vertical droplet incubation chamber and tightly packing them within the chamber, the normally closed pneumatic valve on the fifth layer (L5, Fig. 2f) is opened so that the collected droplets can reflow through the curved droplet transition microstructure (L3 and part of L4) to the fourth layer (L4) by flowing carrier oil from the inlets in the first layer (L1). Here, the third layer (L3) contains a vertically curved chamber-to-channel transition structure to allow smooth droplet transition. The radius of curvature (bottom right curve) is 200 µm (Fig. 1a). In the fourth layer (L4), as the droplets are spaced and accelerated by the introduction of a spacing oil flow (Novec oil 7500 without surfactant), the reflowed droplets cleave a second aqueous flow at the cleaving junction (Fig. 1b) to automatically create paired droplets from

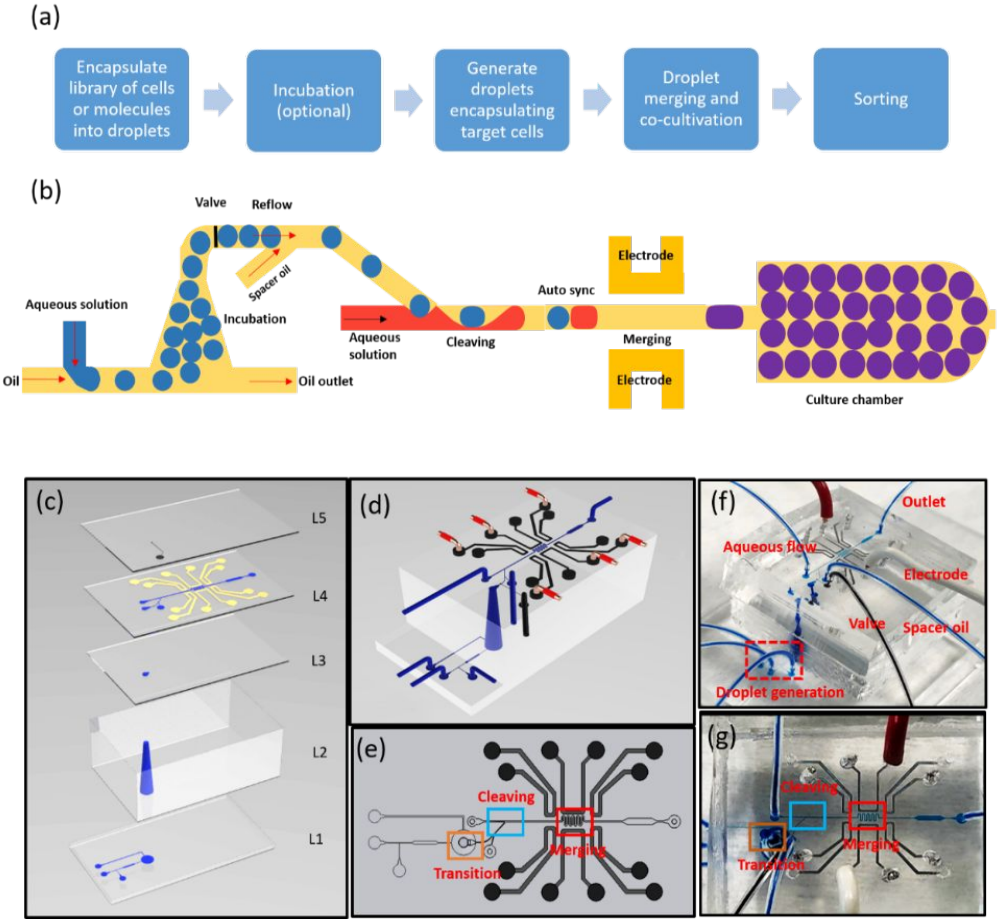

Fig. 2 Schematic and image of the fabricated droplet microfluidic system that can achieve high-efficiency droplet merging utilizing a curved-transition for droplets and auto-synchronized droplet cleaving and merging. (a) The overall workflow of a typical droplet-based assay being realized here. (b) Working principle of the integrated high-efficiency droplet merging platform. (c) Exploded view of each layer of the device. L1: droplet generation; L2: vertical droplet incubation and storage chamber; L3: curved droplet transition structure; L4: curved droplet transition, cleaving, and merging; L5: pneumatic control. (d) 3D illustration of the entire assembly. (e) Top view of the assembly with colored boxes indicating the droplet transition, cleaving, and merging zones. (f) Photographic image (3D view) of the fabricated device, where fluidic channels are filled with blue color dye and pneumatic actual channels are filled with red color dye for easy visualization. (g) Photographic image (top view) of the fabricated device.

this aqueous solution. Then, the one-to-one paired droplets travel to the downstream droplet merging zone (Fig. 1c) and are subsequently merged by an electric field applied by a 3D electrode pair.

2.2 Device fabrication

The device was fabricated by assembling multiple layers of polydimethylsiloxane (PDMS, Sylgard 184 Dow Corning, MI, USA) structures made through a conventional soft lithography fabrication process.[31-34] The master molds for PDMS replication for Layers #1 and #5 were fabricated by conventional photolithography (SU-8 2050TM, MicroChem®, Westborough, MA, USA). The master mold for Layer #2 was fabricated using a 3D stereolithography printer (Perfactory Mini, EnvisionTEC), creating a high aspect ratio structure (8 mm in height, 5mm in diameter) where a resolution of several tens of micrometer was sufficient. The master molds for Layers #3 and #4 were fabricated using a 2PP system (Nanoscribe 3D Photonics Pro GT, Nanoscribe GmbH, Germany) to create the curved structure (in Z-direction) that is needed for the smooth droplet transition scheme developed here. It is to be noted that the additional fabrication processes to produce a curved structure using this instrument does not add significant cost when compared to conventional photolithography processing. The details of the 2PP-based master mold fabrication process are described in more detail in the Electronic Supplementary Information (ESI).

For all PDMS layers (except for Layer #4), the Sylgard 184 base and curing agent were mixed at an 8:1 ratio, stirred vigorously for 5 min, poured onto the master mold, degassed for 30 min under vacuum to remove all air bubbles, and cured at 85 °C for 2 h. The top fluidic channel layer (L4) was spin-coated at 1000 RPM with 2.5 g of PDMS (10:1 ratio of PDMS base vs curing agent) and baked at 85°C for 2 h, resulting in a 200 µm thin layer. The PDMS valve layer (L5) was replicated and placed on top of the PDMS spin-coated channel layer (L4) using methanol-based alignment and bonding. After 2 h baking at 85°C, the normally closed valve was vacuum-actuated using a syringe to keep it open to prevent unexpected bonding of the valve to the PDMS surface, aligned, bonded to the curved chamber outlet layer (L3), and baked overnight at 85°C. This fabrication process results in a normally closed microvalve structure that can be actuated closed/open using pressure/vacuum, respectively. All layers were treated using oxygen plasma at 18 W for 120 s (Harrick Plasma PDC-001-HP) before bonding. The 3D electrode was fabricated by filling the microfluidic electrode channels with Roto 144F Low Melt Fusible Ingot Alloy (Roto Metals, CA, USA) at 85°C, producing 3D electrodes with no additional fabrication steps.[30]

2.3 Experimental setup for evaluating the droplet transition structure

Before the full droplet microfluidic assay system was built, the curved structure-based droplet transition design was first tested, followed by testing the droplet cleaving/pairing/merging scheme. First, for the curved structure-based droplet transition scheme, two identical devices with the only difference being the curved transition zone (conventional step vs. curved) were tested and directly compared (ESI Fig. S1 shows the zoomed-out view of the overall test structure). Both devices consist of two microfluidic layers with identical layer thickness but different microfluidic channel height (200 µm high microchannels in the bottom layer (L3) and 50 µm high microchannels in the top layer (L4)).

Fluorinated oil (Novec 7500, 3M) containing 2 % (wt/wt) surfactant (Pico-Surf™ 2, Sphere Fluidics, Cambridge, UK) was prepared to generate the first water-in-oil emulsion droplets. Color dyes were added to the aqueous solutions for better visualization and analysis of droplet phenomena. Droplets of approximately 60 µm diameter were generated using a T-junction droplet generator (cross-section 50 µm × 50 µm) at a flow rate of 500 µl/h for the oil phase and 100 µl/h for the aqueous phase. The droplets were then flown into a cylindrical-cone shaped droplet cultivation chamber (ESI Fig. S2) similar to that reported in a previous publication[15]. Here, droplets flow from the bottom inlet of this chamber and become tightly packed, since the droplets float up and accumulate in the chamber, while carrier oil flows out through the bottom oil outlet channel. Droplets then reflow out of this chamber through the outlet positioned at the top of this chamber through the droplet transition junction (step-junction vs. curved junction), and then into the top droplet cleaving/merging channel layer. As the packed droplets flow out of the chamber, a spacing oil flow separates the packed droplets to create identical droplet-to-droplet distances. The droplet reflow rate was 20 µl/h, with the spacing oil flow rate being 50 µl/h, resulting in droplets to reflow at a rate of 20 droplets per second.

In this experiment, microscopic images were recorded through a Nikon upright microscope (Eclipse LV 100) equipped with a high-speed CMOS camera (C11440, Hamamatsu) at an image capture rate of 500 frames per second (fps). The time-points at which droplets pass a measurement mark next to the microfluidic channel (Fig. S1) were used for calculating the droplet flow rate. The droplet-to-droplet distance and corresponding time interval were selected as the main investigative criteria since they are affected by both flow speed and droplet size, providing an indication of the stability of the proposed method. In addition, the intactness of the droplets (i.e., no droplet shearing and no unintentional droplet merging) was also measured through microscopic imaging. OriginPro 2018 (v. b9.5.1.195, OriginLab, Northampton, MA, USA) was used for data analysis and plotting.

2.4 Experimental setup for evaluating the integrated droplet cleaving auto-pairing, auto-synchronization and merging method

Droplets generated through the T-junction droplet generator were reflown from the top cone-shaped end of the droplet cultivation chamber, spaced using a spacer oil flow, and then flown into an aqueous flow at an angle of 45˚ (Fig. 1b). This results in the carrier oil of the first droplet train to physically cleave the aqueous stream, creating another set of droplets out of this aqueous solution. Due to the cleaving and generation of

these second sets of droplets by the reflowed droplets, the two droplets are automatically paired one-to-one at an extremely high efficiency. The width of the reflow channel and continuous aqueous phase channel are designed to be 50 µm and 100 µm, respectively, with the height of both channels being 50 µm. The flow rates for the droplet reflow, spacer oil, and aqueous stream were set to 15-20 µl/h, 55-60 µl/h, and 30-35 µl/h, respectively. The overall throughput can be adjusted readily by proportionally adjusting the flow rates. Syringe pumps (Fusion 400, Chemyx Inc.) were used to control volumetric flow rates of all input streams. The images and videos were captured through a microscope using a CMOS camera (C11440, Hamamatsu) for lower frame rates (<1,000 FPS) and a VEO710 ultra-high-speed camera (Phantom, NJ, USA) for higher frame rates (>1,000 FPS). A function generator (DG4102, Rigol) and a high-voltage power amplifier (Model 2210-CE, TREK) were used to applying an electrical field for droplet merging. In most cases, a 120 V 20 kHz square wave was used for generating the electric field for droplet merging.

2.5 Cell and reagents reparation for the mock drug screening application demonstration using the integrated droplet microfluidics system

In a large-library drug screening application, a library of droplets each containing unique molecules of potential interest would be generated, reflowed and merged with a target organism-droplet, and the effect of the molecules on the target organism monitored. Here, such molecules of interest could come from environmental microbial libraries whereby microbes are producing molecules of potential interest, synthetic small molecule libraries, or phage libraries, for example. Mimicking such a process here to demonstrate the proposed device function, droplets that contain antibiotics (gentamicin) were generated, reflowed to cleave an aqueous stream containing a target organism (GFP-*Salmonella*)-producing droplet pairs, merged, incubated, and the resulting droplets analyzed. *Salmonella Typhimurium* was chosen as a model organism for demonstrating the developed system. *Salmonella Typhimurium* (strain ATCC 14028S) engineered with a GFP plasmid (pCM 18) was inoculated in a culture tube containing 3 ml Lysogeny broth (LB) media (Sigma-Aldrich, St Louis, MO, USA) and 50 µg/mL erythromycin, followed by incubation at 37°C overnight. The bacteria culture (OD >1) was then diluted (to OD between 0.2 - 0.25) with LB media before putting into the device as the continuous aqueous flow to be cleaved. Two conditions of water-in-oil emulsion droplets (diameter: 55-60 µm) were prepared, the negative control condition being droplets with LB media only and the treatment condition being droplets containing antibiotics and fluorescent bead (PolyFluor® 407) indicators (for easy visualization). Gentamicin (Sigma-Aldrich, St Louis, MO, USA) was used to serve as a surrogate for an unknown antibiotic that can inhibit bacterial growth, and was diluted with LB media to a final concentration of 1 mg/ml. After droplet merging, this gentamicin concentration is diluted by approximately 3-4 times (depending on the size ratio between the reflowed and cleaved droplets). Approximately 50 µl of 1 µm fluorescent (DAPI) beads (2.5% aqueous suspension, emission max = 407 nm, Polysciences, Inc., PA, USA) were added to the prepared gentamicin solution as the fluorescent indicator of antibiotic. The two droplet populations were mixed at two different ratios: 1 (treatment) to 1 (negative control), and 1 (treatment) to 100 (negative control). A Zeiss® Colibri 7 (Carl Zeiss AG, Germany) microscope with an incubation enclosure was used for conducting 8 h long time-lapse imaging of the final co-incubated droplets and subsequent image analysis. The workflow of the experiment is illustrated in Fig. 3.

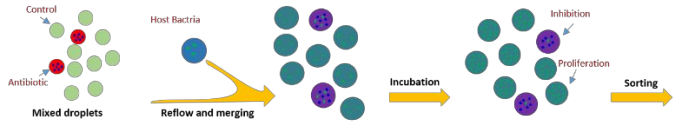

Fig. 3 The assay workflow to conduct a mock antibiotic drug screening application using the high efficiency and high-throughput droplet microfluidic platform developed here.

3. Results and discussion

3.1 Droplet transition through a vertically curved microstructure

Droplets transitioning through the vertically curved microstructures were compared to those transitioning through a step-shaped corner to see whether the curved structure indeed enables a more consistent droplet reflow and minimum droplet disruption (e.g., droplet shearing, droplet splitting and droplet merging). Fig. 4 compares how droplets transition through the vertically curved transition structure in comparison to the conventional step-shaped transition structure. Fig. 4 a – d show the top and side view of the two types of droplet transition junctions that were compared. As is shown in Fig. 4a, the microfluidic channel height gradually changes from 250 µm to 50 µm over a length of 200 µm, creating a curved slope structure. In contrast, Fig. 4b shows a conventional step-shaped transition region where the channel height changes abruptly in a stepwise fashion. In addition, in an effort to minimize the dead volume and eliminate any sharp curves, where such zones can contribute to unwanted droplet merging during droplet transition and cause variations in droplet-to-droplet distances, the top left and bottom right corners were made into curved corners (Fig. 4c, also using a 2PP-fabricated PDMS master mold). The velocity profiles within the droplet transition zones were simulated using the COMSOL Multiphysics® simulation software. The simulation parameters are described in the ESI. The simulated velocity profiles within the droplet transition zones show that the curved transition structure has a more stable flow, smoother flow transition, and less dead volume (ESI Fig. S3 a & b). Also, the velocity profile is more evenly distributed in the curved transition junction (ESI Fig. S3c), compared to that of the traditional step-shaped transition junction (ESI Fig. S3d) where the velocity near the wall is much higher than other places. This higher velocity profile in the step-shaped transition junction indicates that in those regions' droplets will experience higher shear stress, which often contributes to a higher probability of droplet merging or splitting (ESI Video S1).

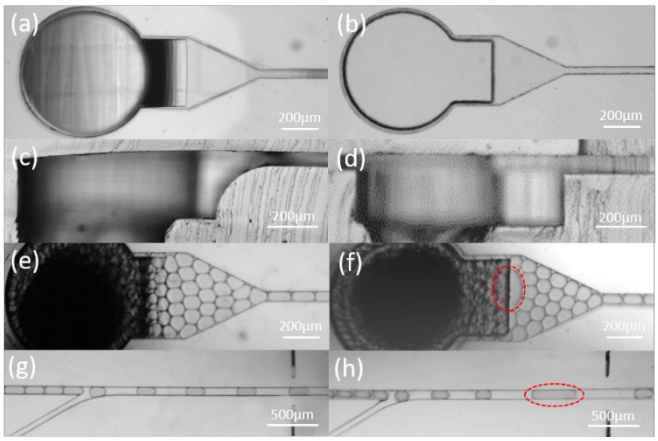

Fig. 4 Micrograph images comparing the vertically curved droplet transition junction to the conventional step-shaped transition junction. Top view of (a) the 2PP-printed vertically curved transition junction and (b) the conventional step-shaped transition junction. Cross-sectional view from the side of the (c) curved transition junction and (d) step-shaped transition junction. Top view of droplets reflowing through the (e) curved transition junction and (f) step-shaped transition junction. In the step-shaped transition junction, some droplet merging occurring can be observed (red circled area of "f"). (g) An example of good droplets reflow out from the droplet incubation chamber and into the straight channel, with spacer oil flow from lower left channel creating distances between the reflowed droplets. No droplet shearing or merging is observed. (f) An example of poor outflow of droplets from the conventional step-shaped junction structure, where droplet-to-droplet distances are inconsistent, and in some cases where merged droplets are seen (red circled area).

Experimentally, both junction structures were evaluated by reflowing droplets (approximately 60 μm in diameter) through the transition zones. The intactness of the droplets (i.e., no unwanted droplet shearing or droplet merging) and droplet-to-droplet distances were examined to compare droplet transition through these two structures. Fig. 4e & f and ESI Video S1 show a direct comparison of droplets reflowing through the entrance part of the droplet transition zones. It can be seen that in the curved transition structure (Fig. 4e), droplets continue to be tightly packed and seen orderly transitioning into the downstream flow channel (from left to right), while in the conventional step-shaped transition structure occasional droplet merging occurs (an example of droplet merging can be observed in the red circled area of Fig. 4f, where such merging occurred at the transition region). Furthermore, it can also be seen that the droplets in the conventional step-shaped transition structure are less tightly packed (indicated by more spacing between droplets observed and less deformed droplet shapes), which results in inconsistent droplet reflow into the downstream flow channel. Ideal and non-ideal examples of droplet reflow downstream are seen in Fig. 4g (from curved transition microstructure) and Fig. 4h (from step-shaped transition microstructure), respectively.

To quantitatively analyze the droplet reflow characteristics in the two different droplet transition structures, the time intervals between droplets passing by a measurement mark were measured and summarized in Table 1. The droplet flow rate was approximately 20 droplets/second. This analysis shows that the relative standard deviation (RSD) of the droplet reflow time interval in the curved transition structure is 7.10%, which is much smaller than the case of the conventional step-shaped transition structure (16.21%). One-way ANOVA test shows that there is a significant statistical difference ($p = 0$). The higher RSD seen in the step-shaped droplet transition zone can be contributed to the abrupt changes in flow direction/speed as droplets compete to enter the microchannel or the appearance of large/small droplets from undesired droplets merging and/or splitting. Undesired droplet merging and/or splitting ratios were zero out of 500 droplets measured (curved transition, 0%) and 9 out of 500 droplets (curved transition, 1.8%).

Table 1 Time interval between each droplet passing the measurement mark (frame rate: 500 fps)

Transition type	Counted droplets	Flow rate (μl/h)	Mean time Interval (s)	RSD (%)
Step shape (conventional)	500	20	0.0547	16.21
Curved shape (this design)	500	20	0.0470	7.10

3.2 High-efficiency droplet cleaving and auto-pairing/auto-synchronization

Droplet pairing plays a vital role in achieving high-efficiency droplet merging. Fig. 5a shows micrographs of packed droplets reflowing with the addition of a spacer oil flow to create a set of distances between the droplets depending on the flow rates. This train of droplets was then flown into the aqueous flow channel at a 45˚ angle and cleaved the aqueous-phase flow to form automatically paired and synchronized droplets (Fig. 5b). Here, a cyan color droplet surrounded by carrier oil physically pinches the brown-color aqueous flow and cleaves the aqueous solution to form a droplet, which is automatically paired and synchronized with the cyan-color droplet. Higher flow rates of the spacer oil lead to larger distances between the cleaving droplets, higher droplet flow speed, and higher momentum for cleaving.

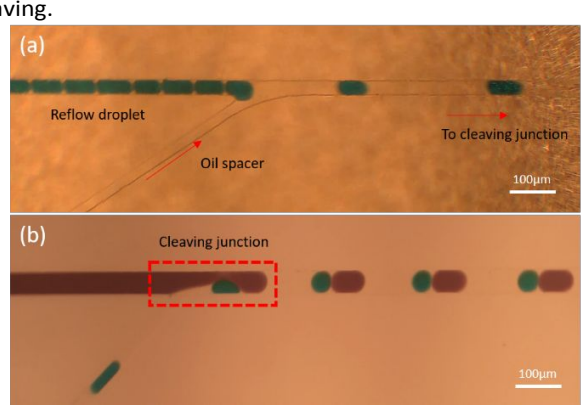

Fig. 5 Micrographs showing high-efficiency droplet pairing using the on-the-fly auto-synchronizing droplet cleaving system. (a) Oil spacer flow adding oil between the reflowed droplets so that the droplets have a fixed droplet-to-droplet distances. (b) One-to-one droplet cleaving and auto-synchronized pairing of droplets.

Fig. 6 shows the effects of changing the aqueous phase flow speed or channel width on the size of the resulting cleaved droplets. The initial flow rates were set to 20 μl/h (droplet

reflow, 2.24 mm/sec), 60 µl/h (spacer oil flow, 6.72mm/sec), and 35 µl/h (aqueous phase flow, 2.59 mm/sec). It can be seen that the cleaved droplet size (i.e., droplet volume) can be easily adjusted as desired by controlling the droplet reflow rate, droplet spacing oil flow rate, aqueous flow rate, and aqueous flow channel width. The aqueous flow rate and cleaved droplet size are shown to be linearly correlated (Fig. 6a, $R^2 = 0.98$). If the flow rate of the aqueous flow remains the same and the aqueous channel width is varied from 50 µm to 100 µm, the cleaved droplet size increases non-linearly and the two variables fit a polynomial model (Fig. 6b). Adjusting the various conditions as stated above allowed the droplet pairing volume to be adjusted between 100 µm to about 250 µm in terms of droplet length. Additional details regarding the impact of flow rate and channel width on the cleaved droplet length can be found in ESI Fig. S4.

In summary, this demonstrates that a sample that is more than two times smaller or four times larger than the original droplet volume can be easily paired for downstream merging, providing droplet merging at broad ranges of volume ratios. This is a major improvement over other droplet merging techniques where the droplet merging efficiencies are highly dependent on the droplet volume ratio[10, 17, 35-37] or pico-injection where typically only a smaller volume can be added to the incoming droplet. [22-28]

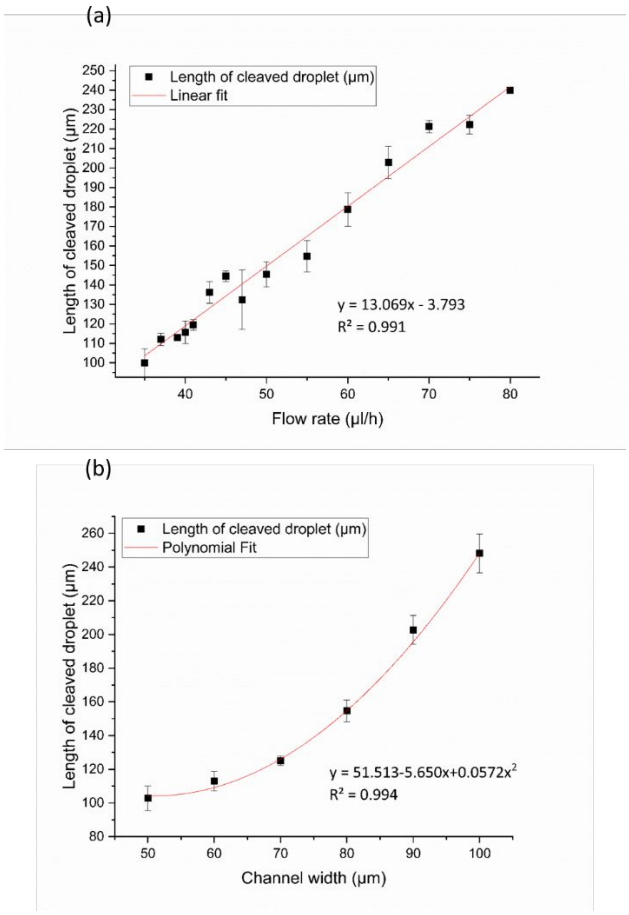

Fig. 6 Graphs showing the effect of the (a) flow rate and (b) channel width on the size of the cleaved droplets using the auto-synchronizing droplet cleaving system ($n = 5$).

Next, droplet cleaving was tested at four different throughputs (from low to high, 4 droplets/sec, 13 droplets/sec (ESI Video S2), 142 droplets/sec, and 1,182 droplets/sec (ESI Video S2)). Frame-by-frame micrograph images showing the entire process of cleaving are shown in Fig. 7. The cleaving and pairing efficiencies were 100%, 98.5%, 100% and 100% ($n = 300$) for the above four throughputs tested, respectively (ESI Fig. S5). Here, missed one-to-one droplet pairing and incorrect ratio pairing (pairing ratio not being one-to-one) are all counted as failed pairing events. An example of a cleaving event error using a conventional step-shaped transition structure is shown in ESI Fig. S6. These results clearly demonstrate that the curved droplet transition junction developed here, together with the new droplet cleaving and auto-synchronization mechanisms, is capable of extremely high-efficiency droplet pairing and merging, providing a practical solution for both low and high flow rate droplet microfluidics applications (throughput ranges from 10 to 1000 events per second).

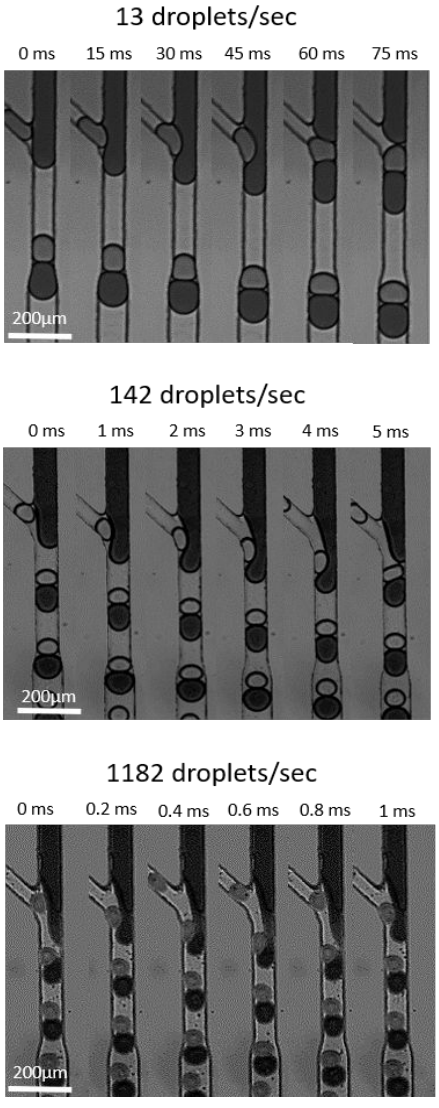

Fig. 7 Frame-by-frame micrograph images of droplet cleaving at different throughputs (13, 142 and 1,182 droplets/sec, respectively) using the curved droplet transition structure with auto-synchronizing droplet cleaving system.

In addition to the reflow rate-dependent cleaving volume control as shown in Fig. 6, in some droplet microfluidics applications, different ratios of droplet pairing, serial pairing, and multi-emulsion pairing may be needed or beneficial, as such capability can provide further flexibility in the biological assays that can be performed in a droplet format. For example, the pairing of different ratios of droplets can be utilized to generate concentration gradients of solutions or cells for dose-response or similar assays. In that regard, Fig. 8 a – d shows that using the developed droplet cleaving scheme, pairing and merging droplets at 1:2, 2:1 (ESI Video 3), 1:3, and 3:1 ratios, beyond just the basic 1:1 ratio, are also possible. Such droplet cleaving methods enable the merging of more than 2 droplets, which can significantly simplify the operation by replacing conventional multiple merging steps into a single cascading merging step, allowing for the realization of complex high-efficiency multi-merging assays. In addition, Fig. 8e shows a serial cleaving scheme that enables droplets containing multiple types of cells or solutions to be paired and merging into one mixed droplet.

In many droplet microfluidic applications, adding objects such as microbeads and cells to the first droplets are also commonly needed[38-40]. Fig. 8f shows the developed droplet cleaving method operating successfully even when the aqueous flow contains relatively large microbeads (29 µm in diameter polystyrene beads). This demonstrates that the developed droplet cleaving method can be broadly utilized even if the aqueous phase contains physical objects such as beads, bacterial cells, and mammalian cells, for example. Taken together, the developed method can be utilized for an extremely broad range of droplet merging scenarios.

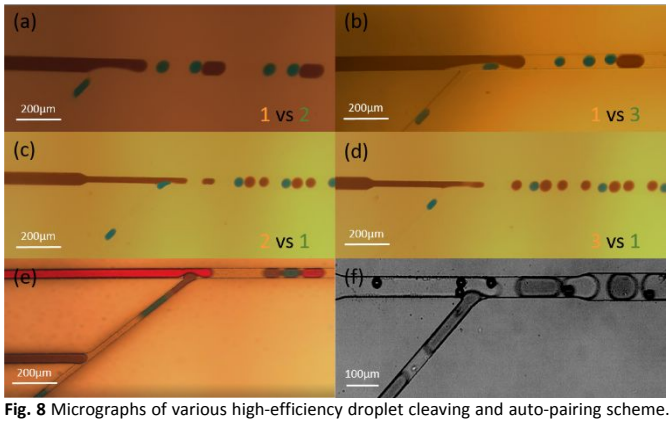

Fig. 8 Micrographs of various high-efficiency droplet cleaving and auto-pairing scheme. (a-b) Different ratios (1 vs 2 (a) and (1 vs 3) (b)) droplet cleaving and pairing by adjusting the droplet reflow, spacer oil, and aqueous flow rates. (c-d) Inverse different ratios (2 vs 1 (c) and (3 vs 1) (d)) droplet cleaving and pairing by adjusting the channel width as well as droplet reflow, spacer oil, and aqueous flow rates. (e) Serial cleaving for pairing multiple droplets. (f) Droplet cleaving and pairing when the aqueous flow contains polystyrene microbeads (diameter = 29 µm).

3.3 Electrical field-based droplet merging of the paired droplets

Automatically paired and synchronized droplets then flowed into the downstream droplet merging region where they were merged by applying an electrical field. Fig. 9 shows the paired droplets in the merging region without and with the application of an electrical field (AC square wave at 120 Volts and 20 kHz applied), respectively. Complete one-to-one droplet merging was observed at the merging region (Fig. 9b) and the resulting merged droplets are shown in Fig. 9d. Here, a meandering channel design was utilized to allow for the droplet dipole moments to be aligned with the electric field multiple times, leading to a greater chance for droplet merging, ensuring that every single pair of droplets are merged before exiting the merging region. These droplet merging tests were conducted at several different flow rates. A final merging efficiency of up to 99.9% was achieved (ESI Video S4), even at the maximum throughput tested of approximately 200 droplets/seconds (ESI Fig. S5). Based on the experimental results, as expected the entire system performs better at higher droplet speed. The possible reason for this is that droplet reflow is slightly less stable at lower flow rate, which also affects the droplet merging efficiency at lower flow speed.

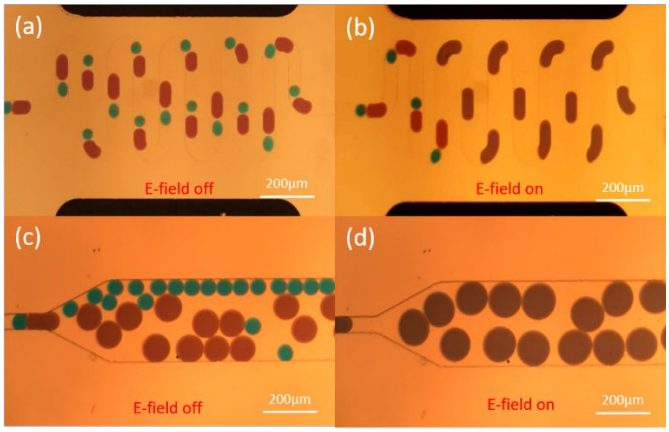

Fig. 9 Micrographs of (a) non-merged droplets and (b) merged droplets in the merging region between the two three-dimensional electrodes (top and bottom black lines) generating an electrical field (120V, 20KHz) and resulting (c) non-merged and (d) merged droplets shown in the downstream observation chamber.

3.4 High-throughput cellular assay example using the developed system

To demonstrate the utility of the developed droplet reflow and droplet merging methods, we have integrated the components into a single comprehensive ultra-high-throughput droplet microfluidic system, as shown in Fig. 2. Fig. 2e and g show the 3D and top views of the integrated platform, where microchannels were filled with color dye for better visualization of the various parts. Using this system, a mock antibiotic drug screening experiment was conducted, following the assay sequence shown in Fig. 3. Fig. 10b shows the final merged droplets, after the droplet generation, reflow, cleaving, and merging processes, collected and cultured in a monolayer basket-like droplet trapping chamber (Fig. 10a) [41] for easy droplet observation and analysis. As can be seen, GFP-*Salmonella* grew to confluency in the negative control condition (having only LB media), where the GFP fluorescence in the droplets increased significantly over the 8 h culture period (Fig. 10b second row). On the contrary, the growth of GFP-*Salmonella* was inhibited under the antibiotic condition where no visible increase in GFP signal was observed (Fig.10b first row).

Next, droplets containing only LB media and droplets containing antibiotics were mixed at 1:1 ratio and then at 1:100 ratio to conduct a mock screening assay simulating an antibiotic discovery functional assay. Microscopic images shown in Fig. 10b third and fourth row demonstrate that for both ratios tested (1:1 and 1:100), all the DAPI-positive droplets (i.e., indicate the existence of antibiotic in that particular droplet) showed no increase in GFP intensity, meaning that the antibiotic successfully suppressed the growth of GFP-*Salmonella*, while all the DAPI-negative droplets showed high GFP intensity after the 8 h culture. The droplet GFP intensity of the control and treatment groups were clearly distinct (ESI Table S1). Statistically, the Z score was calculated[42] to be 0.214 (1:1 droplet mixing ratio, *n = 50*) and 0.201 (1:100 droplet mixing ratio, *n = 50*). The data variability bands can be separated at a 99.73% confidence limit, which indicates that the assay is statistically sound for screening applications.[42] Microscopic images of this experiment using the developed droplet microfluidic system are shown in ESI Fig. S7, Table S1 and Video S4.

Fig. 10 Proof of concept demonstration of the droplet microfluidic system in conducting a mock screening assay. (a) A microscopic image of the pillar-based basket droplet trapping and incubation chamber for monolayer droplet observation. The device filled with blue color dye-encapsulated droplets (left). Bright-field image showing a packed monolayer of droplets in the basket-shaped droplet trapping chamber (right). (b) Droplets before and after the 8 h incubation step. DAPI channel for identifying antibiotic-containing droplets, where strong blue color indicates the presence of antibiotics in the droplet since DAPI beads were co-encapsulated with antibiotics. GFP filter for visualizing the number of cells in the droplets. First and second row: Micrographs of merged droplets where antibiotic-containing droplets show no growth of GFP-*Salmonella* (row one) and LB-containing droplets show extensive growth of GFP-*Salmonella* (row two). Third and fourth row: Antibiotic- and LB-containing droplets mixed at 1: 1 and 1: 100 ratios, respectively (row 3, row 4). It can be clearly seen that in the DAPI-positive droplets minimum growth of GFP-*Salmonella* is observed, while DAPI-negative droplets show exponential growth of GFP-*Salmonella*.

The overall system-level efficiency achieved using the integrated droplet microfluidics platform was 99.9% (less than 0.1% error rate in droplet operation). In a scenario where a library containing 1 million cells have to be screened at a single-cell resolution, a 0.1% error rate means that there will be only 1,000 unmerged/miss-merged droplets. In contrast, a platform that runs at 90% efficiency will result in 100,000 - 200,000 unmerged/miss-merged droplets, which can severely impact the downstream processes such as droplet sorting by causing numerous false positives and false negative cases. In the case of a platform that runs at 99% efficiency, such operations will produce 10,000 - 20,000 unmerged/miss-merged droplets, which is still a very large number considering most assays require time consuming post-processing plate-based confirmation assays. In summary, our novel microfluidic system comprises a fully integrated platform capable of high-efficiency processing for large volume droplet assays with a significantly reduced number of false negatives and false positives.

4. Conclusion

The work herein describes a novel droplet reflow, pairing, and merging method that allows highly efficient and error-resistant automatic droplet synchronization and merging, which was then integrated into a droplet microfluidic screening system and demonstrated through a mock screening assay. A curved two-photon photolithography fabricated vertical curved transition layer was integrated to allow for a smooth transition of droplets between adjacent layers. This vertically curved droplet transition junction was validated to show highly consistent droplet reflow, outperforming conventional photolithography-based fabricated step-shaped droplet transition structures under identical experimental conditions. In addition, a novel droplet cleaving approach where reflowed droplets physically cleave a secondary aqueous flow stream at an acute-angled Y-junction led to the automatic pairing of droplets at an ultra-high efficiency. The developed droplet reflow and droplet cleaving/auto-synchronization method were combined with a three-dimensional electrode-based droplet electrocoalescence design, and resulted in a one-to-one droplet merging efficiency of 99.9%. Simply changing various operating conditions and microstructure dimensions allowed the droplet

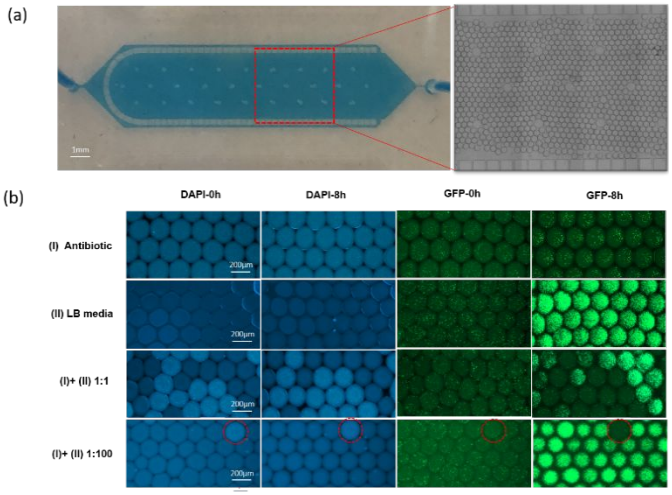

merging ratios and cleaved droplet sizes to be controlled in a desired manner. The method could also be applied to cleave and merge microbead or large cell-containing aqueous streams. Linking two droplet cleaving structures in series also enabled more complex droplet merging operations. Integrating these methods into a droplet microfluidic screening platform, a proof of concept mock drug screening assay was successfully conducted using *Salmonella* as the target cell. Up until now the development of integrated droplet microfluidic-based platforms has been hindered by the difficulty in conducting sequential on-chip manipulation of droplets with high-efficiency. We expect that the presented technology can lead to enabling wide ranges of complex multi-step droplet assays to be performed. The extremely simple microstructure and method allow this new technology to be integrated into broad ranges of droplet microfluidics-based screening applications especially when multiple sequential assay steps are required and where a relatively large library has to be screened, and thus can have broad implications on the field of droplet microfluidics.

Author contributions

A.H., H.Z., and A.G. conceived the project. H.Z., A.G., Y.L., J.W., J.D. and C.H. designed and carried out experiments and analyzed the data. All authors contributed to writing the manuscript.

Conflicts of interest

A provisional patent has been filed by the institute.

Acknowledgments

The project depicted is sponsored by the Defense Advanced Research Projects Agency (Agreement W911NF1920013). The content of the information does not necessarily reflect the position or the policy of the Government, and no official endorsement should be inferred. J. Wippold was supported through the Department of Defense Graduate SMART Scholarship program.

References

1. S. Cho, D.-K. Kang, S. Sim, F. Geier, J.-Y. Kim, X. Niu, J. B. Edel, S.-I. Chang, R. C. R. Wootton, K. S. Elvira and A. J. deMello, *Analytical Chemistry*, 2013, **85**, 8866-8872.
2. J. Clausell-Tormos, D. Lieber, J.-C. Baret, A. El-Harrak, O. J. Miller, L. Frenz, J. Blouwolff, K. J. Humphry, S. Köster and H. Duan, *Chemistry & Biology*, 2008, **15**, 427-437.
3. B. El Debs, R. Utharala, I. V. Balyasnikova, A. D. Griffiths and C. A. Merten, *Proceedings of the National Academy of Sciences*, 2012, **109**, 11570-11575.
4. M. Sesen, T. Alan and A. Neild, *Lab on a Chip*, 2017, **17**, 2372-2394.
5. L. Shang, Y. Cheng and Y. Zhao, *Chemical reviews*, 2017, **117**, 7964-8040.
6. A. M. Kaushik, K. Hsieh and T. H. Wang, *Wiley Interdisciplinary Reviews: Nanomedicine and Nanobiotechnology*, 2018, **10**, e1522.
7. R. Tewhey, J. B. Warner, M. Nakano, B. Libby, M. Medkova, P. H. David, S. K. Kotsopoulos, M. L. Samuels, J. B. Hutchison and J. W. Larson, *Nature biotechnology*, 2009, **27**, 1025.
8. X. Niu, S. Gulati, J. B. Edel and A. J. deMello, *Lab on a Chip*, 2008, **8**, 1837-1841.
9. K. Ahn, J. Agresti, H. Chong, M. Marquez and D. A. Weitz, *Applied Physics Letters*, 2006, **88**, 264105.
10. B. Ahn, K. Lee, H. Lee, R. Panchapakesan and K. W. Oh, *Lab on a Chip*, 2011, **11**, 3956-3962.
11. L. Shui, J. C. T. Eijkel and A. van den Berg, *Advances in Colloid and Interface Science*, 2007, **133**, 35-49.
12. M. T. Chung, D. Núñez, D. Cai and K. Kurabayashi, *Lab on a Chip*, 2017, **17**, 3664-3671.
13. N. Shembekar, H. Hu, D. Eustace and C. A. Merten, *Cell reports*, 2018, **22**, 2206-2215.
14. B. Kintses, L. D. van Vliet, S. R. A. Devenish and F. Hollfelder, *Current Opinion in Chemical Biology*, 2010, **14**, 548-555.
15. J. Dai, H. S. Kim, A. R. Guzman, W.-B. Shim and A. Han, *RSC advances*, 2016, **6**, 20516-20519.
16. B. O'Donovan, T. Tran, A. Sciambi and A. Abate, *JoVE (Journal of Visualized Experiments)*, 2014, e50913.
17. Y. Qiao, J. Fu, F. Yang, M. Duan, M. Huang, J. Tu and Z. Lu, *RSC advances*, 2018, **8**, 34343-34349.
18. R. Chen, Z. Sun and D. Chen, in *Microfluidics for Pharmaceutical Applications*, Elsevier, 2019, pp. 307-335.
19. D. M. Headen, J. R. García and A. J. García, *Microsystems & Nanoengineering*, 2018, **4**, 1-9.
20. M. T. Guo, A. Rotem, J. A. Heyman and D. A. Weitz, *Lab on a Chip*, 2012, **12**, 2146-2155.
21. H. N. Joensson and H. Andersson Svahn, *Angewandte Chemie International Edition*, 2012, **51**, 12176-12192.
22. B. O'Donovan, D. J. Eastburn and A. R. Abate, *Lab on a Chip*, 2012, **12**, 4029-4032.
23. A. R. Abate, T. Hung, R. A. Sperling, P. Mary, A. Rotem, J. J. Agresti, M. A. Weiner and D. A. Weitz, *Lab on a Chip*, 2013, **13**, 4864-4869.
24. H. Yuan, Y. Pan, J. Tian, Y. Chao, J. Li and H. C. Shum, *Sensors and Actuators B: Chemical*, 2019, **298**, 126766.
25. A. R. Abate, T. Hung, P. Mary, J. J. Agresti and D. A. Weitz, *Proceedings of the National Academy of Sciences*, 2010, **107**, 19163-19166.
26. D. J. Eastburn, A. Sciambi and A. R. Abate, *PloS one*, 2013, **8**, e62961.
27. H. Yuan, Y. Chao, S. Li, M. Y. Tang, Y. Huang, Y. Che, A. S. Wong, T. Zhang and H. C. Shum, *Analytical chemistry*, 2018, **90**, 13173-13177.
28. M. Rhee, Y. K. Light, S. Yilmaz, P. D. Adams, D. Saxena, R. J. Meagher and A. K. Singh, *Lab on a Chip*, 2014, **14**, 4533-4539.
29. A. Sciambi and A. R. Abate, *Biomicrofluidics*, 2013, **7**, 044112.
30. A. R. Guzman, H. S. Kim, P. de Figueiredo and A. Han, *Biomedical microdevices*, 2015, **17**, 35.
31. H. Chen, J. Cornwell, H. Zhang, T. Lim, R. Resurreccion, T. Port, G. Rosengarten and R. E. Nordon, *Lab on a Chip*, 2013, **13**, 2999-3007.
32. M. A. Unger, H.-P. Chou, T. Thorsen, A. Scherer and S. R. Quake, *Science*, 2000, **288**, 113-116.
33. H. Zhang, W. Zhang, L. Xiao, Y. Liu, T. A. Gilbertson and A. Zhou, *Sensors*, 2019, **19**, 1663.
34. J. A. Wippold, H. Wang, J. Tingling, J. L. Leibowitz, P. de Figueiredo and A. Han, *Lab on a Chip*, 2020.
35. L. Shui, J. C. Eijkel and A. van den Berg, *Advances in colloid and interface science*, 2007, **133**, 35-49.
36. J. Köhler, T. Henkel, A. Grodrian, T. Kirner, M. Roth, K. Martin and J. Metze, *Chemical Engineering Journal*, 2004, **101**, 201-216.
37. B. Demaree, D. Weisgerber, F. Lan and A. R. Abate, *JoVE (Journal of Visualized Experiments)*, 2018, e57598.
38. E. Brouzes, M. Medkova, N. Savenelli, D. Marran, M. Twardowski, J. B. Hutchison, J. M. Rothberg, D. R. Link, N. Perrimon and M. L. Samuels, *Proceedings of the National Academy of Sciences*, 2009, **106**, 14195-14200.
39. S. Köster, F. E. Angile, H. Duan, J. J. Agresti, A. Wintner, C. Schmitz, A. C. Rowat, C. A. Merten, D. Pisignano and A. D. Griffiths, *Lab on a Chip*, 2008, **8**, 1110-1115.
40. J. F. Edd, D. Di Carlo, K. J. Humphry, S. Köster, D. Irimia, D. A. Weitz and M. Toner, *Lab on a Chip*, 2008, **8**, 1262-1264.
41. H. S. Kim, A. R. Guzman, N. Sobahi, H. R. Thapa, T. P. Devarenne and A. Han, High-throughput droplet-based screening system for investigating microalgae library, 2015.

42. J.-H. Zhang, T. D. Chung and K. R. Oldenburg, *Journal of biomolecular screening*, 1999, **4**, 67-73.